Physics of the Earth and Planetary Interiors 180 (2010) 235–243

Contents lists available at ScienceDirect

Physics of the Earth and Planetary Interiors

journal homepage: www.elsevier.com/locate/pepi

Implications of post-perovskite transport properties for core–mantle dynamics

Hana Čížková[a,*], Ondřej Čadek[a], Ctirad Matyska[a], David A. Yuen[b]

[a] Charles University in Prague, Faculty of Mathematics and Physics, Department of Geophysics, V Holešovičkách 2, 180 00 Praha 8, Czech Republic
[b] University of Minnesota, Department Geology and Geophysics and Minnesota Supercomputing Institute, Minneapolis, USA

ARTICLE INFO

Article history:
Received 1 April 2009
Received in revised form 6 August 2009
Accepted 11 August 2009

Guest Editors
Kei Hirose
Thorne Lay
David Yuen

Editor
G. Helffrich

Keywords:
Post-perovskite
Dislocation creep
D″
CMB heat flux
Mantle convection

ABSTRACT

Recent evidence on perovskite to post-perovskite phase change in the lowermost mantle suggests that post-perovskite piles or lens should be present in the relatively cold downwelling areas, while the roots of the hot upwelling plumes consist of perovskite. Post-perovskite is often believed to be deformed predominantly by the dislocation creep and there are some hints that the activation parameters of the dislocation creep in post-perovskite induce lower viscosity than that of perovskite at the same pressure and temperature conditions. That can even result in a viscosity paradox in the lowermost mantle—viscosity in cold downwellings transformed to post-perovskite might be lower than the viscosity of warm perovskite plumes. Such a viscosity structure was indeed recently suggested by the geodynamical inversions of the geoid. Rheologically weak areas at the base of the subducted slabs may have important consequences for the slab deformation in the *D″*. We investigate the dynamics of the cold slabs transformed to post-perovskite in the lowermost mantle by means of the simulations of thermal convection in a 2D Cartesian model of the lower mantle with composite rheology including diffusion creep and dislocation creep. Different creep parameters are used for the perovskite lower mantle and for the post-perovskite lens (or layer) respectively. While perovskite is considered to be deformed via linear diffusion creep, post-perovskite is modeled either as a constant viscosity material (with viscosity ranging from 10^{20} Pa s to 10^{23} Pa s) or it is deformed purely by the dislocation creep. The presence of the rheologically distinct post-perovskite not only strongly influences the slab deformation above the core–mantle boundary (CMB) but also results in different dynamic regimes of the CMB region (characterised by, e.g., the different length scales of the upwelling plumes) depending on the creep parameters of post-perovskite. Further, the presence of very low viscosity lens or a layer above the CMB strongly enhances the CMB heat flux in the cold slab areas. According to the amount of post-perovskite present in the *D″* and the rheology of post-perovskite the heat flux across the CMB can vary considerably with time, which may have important implications for the core–mantle coupling and the character of the Earth's geomagnetic field.

1. Introduction

The lowermost layer of the Earth's mantle, the *D″*, has been subject to investigations for past few years. The complex structure and dynamic processes occurring in this thermo-chemical boundary layer received a lot of attention and many scenarios of its development have been suggested. Recently, an interest in this particular mantle region has been promoted by the discovery of the new high-pressure phase—the post-perovskite (Murakami et al., 2004; Oganov and Ono, 2004; Tsuchiya et al., 2004). The exothermic phase change of perovskite to post-perovskite has been reported to occur several hundred kilometers above the CMB. The large Clapeyron slope of this exothermic phase change – about 9 MPa/K – should yield large lateral variations of the boundary depth or even disappearance of the post-perovskite in the hot plume root regions. Moreover, the steep vertical thermal gradients in the bottom boundary layer should result in a double crossing of the phase boundary and thus the existence of the isolated post-perovskite lens has been predicted (Hernlund et al., 2005) and later even supported by seismic observations (van der Hilst et al., 2007); see also the discussion by, e.g., Hirose and Lay (2008); Shim (2008). The presence of the post-perovskite piles both overlain and underlain by perovskite is not only very important for constraining the mantle geotherm, but could also have a strong influence on the lowermost mantle dynamics, provided that the transport properties of post-perovskite are not the same as those of perovskite (e.g., Yuen et al., 2007). The electrical conductivity of post-perovskite has been reported to be significantly higher than that of perovskite (Ono et al., 2006; Ohta et al., 2008). Similarly, there are some hints, that the viscosity may differ considerably between the perovskite and the post-perovskite.

* Corresponding author. Tel.: +420 2 2191 2544; fax: +420 2 2191 2555.
E-mail address: hk@karel.troja.mff.cuni.cz (H. Čížková).

0031-9201/$ – see front matter © 2009 Elsevier B.V. All rights reserved.
doi:10.1016/j.pepi.2009.08.008

Though the precise determination of the post-perovskite rheology is still a task for future research, there are several indications that may help to constrain the model of the lowermost mantle deformation. The lack of the seismic anisotropy observations in the bulk of the lower mantle is generally interpreted as the evidence of the predominantly diffusion creep deformation of the perovskite (Yamazaki and Karato, 2001). On the other hand, the lattice preferred orientation observed in the bottom boundary layer indicates that in the *D″* the role of the dislocation creep is dominant (Karato, 1998; Yamazaki et al., 2006). This hypothesis is supported by several other evidences coming from both the first principle calculations (Oganov and Ono, 2005; Carrez et al., 2007) and the experiments carried out on the $CaIrO_3$ perovskite and post-perovskite (Walte et al., 2007). There are certain indications, that the yield strength difference between the perovskite and post-perovskite may be as high as 2–3 orders of magnitude (A. Oganov, personal communication). We should emphasize, however, that our knowledge of the post-perovskite rheology is far from being robust and some of the estimates mentioned above may be affected by the application of an inaccurate theory or by the low temperature of the experiments, as discussed by Yamazaki and Karato (2007). Another physical mechanism that might significantly decrease the viscosity of post-perovskite in comparison with that of perovskite is the weakening of the diffusion creep due to the grain size reduction (for general discussion of the grain-size sensitive creep, see, e.g. Karato et al., 1995; Solomatov, 1996; Yamazaki et al., 1996; Riedel and Karato, 1997; Solomatov et al., 2002). The change in the grain size due to the perovskite to-post-perovskite phase transition may lead to a significant weakening of the slabs which would have important implication for their deformation and influence the long-wavelength geoid considerably (Tosi et al., 2009).

Moreover, it could explain a viscosity paradox found in the recent geoid inversions. Čadek and Fleitout (2006), who inverted the geoid to constrain the lateral viscosity structure just above the CMB, report on the first look contraintuitive viscosity pattern within the *D″*. They observe relatively high viscosity under the hotspot areas, while, unexpectedly, low viscosity turns out below the areas of paleosubductions. Such a pattern can be explained, if we assume that the post-perovskite lens formed in the cold slabs are much weaker, than the neighbouring perovskite plumes (Fig. 1), as was suggested by Yuen et al. (2007). It should be mentioned, however, that Čadek and Fleitout (2006) assumed that the seismic velocity anomalies in the mantle are of thermal origin and considered only positive values of the velocity-to-density scaling factor when performing the inversion. As suggested in numerous studies (Ishii and Tromp, 1999; Masters et al., 2000; Karato and Karki, 2001), the velocity variation in some parts of the mantle may be due to chemical heterogeneity, although some other studies (e.g. Forte and Mitrovica, 2001; Forte et al., 2002) argue for mostly positive correlation between the seismic velocity variations and the density anomalies driving the flow in the mantle. In spite of the large uncertainty in the model given by Čadek and Fleitout (2006), we believe that the viscosity distribution presented there for the core–mantle boundary region may reflect basic rheological properties of material in the lowermost mantle and it is worth further testing.

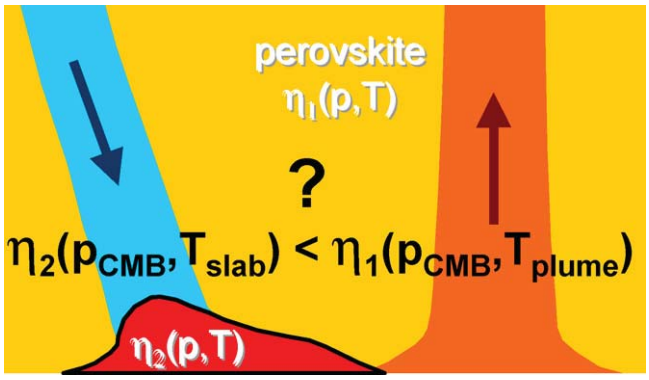

Fig. 1. Schematic chart of the possible lowermost mantle viscosity distribution. A cold downwelling slab (blue) to the left transforms to post-perovskite (red pile), while the upwelling plume on the right (orange) consists of perovskite. (For interpretation of the references to color in this figure legend, the reader is referred to the web version of the article.)

Fig. 2. Sketch of the model domain with the indication of the boundary conditions.

In the present paper we study the dynamics of the slabs in the lowermost mantle by means of the numerical simulations of the thermal convection. We consider the perovskite to post-perovskite phase transition and assume, that the rheological description of the post-perovskite differs from that of the perovskite. Since the rheology of post-perovskite is not well constrained so far, we perform a parametric study and test several values of post-perovskite activation parameters as well as the characteristics of the perovskite to post-perovskite phase change, namely the temperature intercept. We test, whether the scenario of the low viscosity lens under the cold slabs surrounded by the (relatively) high viscosity perovskite plumes is dynamically feasible. Further, we explore how the rheologically distinct post-perovskite influences the dynamics of the *D″* region, especially the size of the plumes, their activity and the heat transport from the core.

2. Model

To study the dynamics of the slabs in the lowermost mantle, we have performed the numerical simulations in a 2D Cartesian finite element model. We have used the extended Boussinesq approximation (including the viscous and adiabatic heating) with an infinite Prandtl number (Ita and King, 1994). We have solved the equations of the mass, momentum and energy conservation (for the details see, e.g. van Hunen et al., 2000) using the finite element package SEPRAN (Segal and Praagman, 2005).

Our rectangular model domain spans the lower mantle—its upper boundary thus represents the boundary at the 660 km depth and the lower boundary is the CMB. The domain is 2240 km deep and its aspect ratio is five. At the bottom and both sides the impermeable free-slip boundary conditions are prescribed. The top boundary is divided into three parts: two 3400 km long segments located in the left and right hand parts of the top boundary (Fig. 2), where the influx is prescribed and the central part, where free outflux is assumed. The influx parts of the boundary allow us to prescribe two slabs sinking into the lower mantle, one positioned 1800 km far from the left-hand corner, the other one 2200 km from the right-hand corner. Both slabs are modeled as a Gaussian shape anomaly with a halfwidth of 150 km and the maximum temperature contrast of 800 K with respect to the ambient mantle. The temperature boundary conditions are as follows: at the bottom, a constant temperature of 4000 K is prescribed, while at the influx parts of the upper boundary we have the temperature of 1900 K which drops to 1100 K at the places, where the slabs are located. Thus we have a constant influx of cold material at two fixed positions with the influx velocity of 3 cm/yr. At the verti-

cal sides and at the free outflux part of the top a zero heat flux is prescribed. The initial temperature distribution is obtained by running a short initial run with the above mentioned temperature boundary conditions, but with the impermeable free-slip on all boundaries. This allows us to develop a temperature distribution in the bottom thermal boundary layer, which is consistent with the model rheology. At the beginning of our model runs we thus have two cold slabs subducted to about one-third of the lower mantle and a developed plume in the bottom boundary layer.

Rheological description of the mantle material often assumes a composite model (van den Berg et al., 1993), where the diffusion and dislocation creep are combined and the effective viscosity is

$$\frac{1}{\eta_{\mathrm{eff}}} = \frac{1}{\eta_{\mathrm{diff}}} + \frac{1}{\eta_{\mathrm{disl}}}.$$

The viscosities of the diffusion and the dislocation creep follow the Arrhenius law:

$$\eta_{\mathrm{diff}} = A_{\mathrm{diff}}^{-1} exp\left(\frac{E_{\mathrm{diff}} + pV_{\mathrm{diff}}}{RT}\right),$$

$$\eta_{\mathrm{disl}} = A_{\mathrm{disl}}^{-1/n} \dot{\epsilon}^{(1-n)/n} exp\left(\frac{E_{\mathrm{disl}} + pV_{\mathrm{disl}}}{nRT}\right).$$

The list of used symbols is given in Table 1. As perovskite is supposed to deform purely by diffusion creep, we assume, that in perovskite $\eta_{\mathrm{eff}} = \eta_{\mathrm{diff}}$. Since the rheological parameters of perovskite are not very well constrained, we test two sets of activation parameters. The first one with relatively low values of the activation parameters is motivated by the results of Knittle and Jeanloz (1987), who report low values of the activation parameters of back transformation of perovskite. The prefactor A_{diff} was taken such as to produce a reasonable value of the lower mantle viscosity (ranging between 10^{22} Pa s and 10^{23} Pa s). The second set has somewhat higher activation energy and activation volume. Those were derived on the basis of the paper by Yamazaki and Karato (2001), by fitting their viscosity curves. What concerns post-perovskite, the rheological parameters are even less constrained. We assume that post-perovskite deforms via dislocation creep and $\eta_{\mathrm{eff}} = \eta_{\mathrm{disl}}$ in post-perovskite. The activation parameters are however not known. We have some indications that the viscosity of post-perovskite may be by up to 2–3 orders of magnitude lower than the viscosity of perovskite under the same pressure and temperature conditions. Since we have no information about the activation parameters, we take the activation energy and activation volume of dislocation creep in post-perovskite equal to the diffusion creep activation parameters of perovskite. The prefactor A_{disl} is then chosen to produce the post-perovskite viscosity approximately 2 orders of magnitude weaker than that of perovskite. The power-law exponent n is equal to 4 in all calculations. In addition to the above mentioned models, we also test a simplified model, where the perovskite is deformed via diffusion creep with pressure and temperature dependent viscosity, while the post-perovskite is even simpler—it deforms via diffusion creep with a constant viscosity. We thus have the following sets of rheological parameters: (1) set RKJ, where the activation parameters based on Knittle and Jeanloz (1987) are used for the perovskite and the post-perovskite is not taken into account, (2) set RKJ-C with the same perovskite parameters, while post-perovskite has a constant viscosity ranging between 10^{20} Pa s and 10^{22} Pa s, (3) set RKJ-PL with a perovskite based again on Knittle and Jeanloz (1987) and a corresponding power-law post-perovskite and (4) set RYK-PL with the perovskite parameters based on Yamazaki and Karato (2001) and a corresponding power-law post-perovskite (see Table 2).

Table 1
Symbols used in the rheological description.

Symbol	Meaning	Units
A_{diff}	Pre-exponential parameter of diffusion creep	$\mathrm{Pa}^{-1}\,\mathrm{s}^{-1}$
A_{disl}	Pre-exponential parameter of dislocation creep	$\mathrm{Pa}^{-n}\,\mathrm{s}^{-1}$
E_{diff}	Activation energy of diffusion creep	$\mathrm{J\,mol}^{-1}$
E_{disl}	Activation energy of dislocation creep	$\mathrm{J\,mol}^{-1}$
n	Viscosity stress exponent	–
R	Gas constant	$\mathrm{J\,K}^{-1}\,\mathrm{mol}^{-1}$
T	Temperature	K
P	Hydrostatic pressure	Pa
V_{diff}	Activation volume of diffusion creep	$\mathrm{m}^3\,\mathrm{mol}^{-1}$
V_{disl}	Activation volume of dislocation creep	$\mathrm{m}^3\,\mathrm{mol}^{-1}$
$\dot{\epsilon}$	Second invariant of the strain rate	s^{-1}

Table 2
Activation parameters of individual models.

Model	Perovskite		Post-perovskite	
RKJ	A_{diff}	1×10^{-20}		
	E_{diff}	9×10^{4}	no PPv	
	V_{diff}	1×10^{6}		
RKJ-C	A_{diff}	1×10^{-20}		
	E_{diff}	9×10^{4}	$\eta_{PPv} = 10^{20}$to10^{22}	
	V_{diff}	1×10^{6}		
RKJ-PL	A_{diff}	1×10^{-20}	A_{disl}	1×10^{-39}
	E_{diff}	9×10^{4}	E_{disl}	9×10^{4}
	V_{diff}	9×10^{4}	V_{disl}	1×10^{-6}
			n	4
RKJ-PL	A_{diff}	1×10^{-18}	A_{disl}	1×10^{-37}
	E_{diff}	1.5×10^{5}	E_{disl}	1.5×10^{5}
	V_{diff}	2.5×10^{-6}	V_{disl}	2.5×10^{-6}
			n	4

The phase change of the perovskite to post-perovskite is characterised by two parameters—intercept temperature and Clapeyron slope. The latter is taken to be constant in all calculations (9 MPa/K). In most of our calculations we assume the intercept temperature of 3500 K, we however test the influence of this parameter by varying it in the range 3300–4200 K. The phase transition is parameterised with a harmonic phase function Γ (van Hunen et al., 2004) with the transition width being 10 km. Both buoyancy and latent heat effects of the phase transition are taken into account.

3. Results

We will now discuss the results obtained for the different parameters of the post-perovskite phase transition and the different rheological models. For each model we will show one snapshot taken after 350 Myr evolution from the initial state. Fig. 3 shows three models: RKJ without post-perovskite (panel a), the model RKJ-C with a constant viscosity post-perovskite (10^{21} Pa s) (panel b), and model RKJ-PL with a power-law rheology of post-perovskite (panel c). Each panel shows the distribution of the temperature (upper row) and the logarithm of viscosity (lower row). The model where the post-perovskite phase transition is not considered (Fig. 3a) is characterised by two downwelling slabs and one plume between them. When the slabs reached the CMB, they were deflected towards each other (resembling two ice-hockey sticks) and pushed the warm material between them to form an upwelling plume. The thermal anomaly associated with the cold slabs lying flat in the D'' is quite strong – about 500 K – and induces the high viscosity (over 10^{23} Pa s) in these areas. The viscosity in the central plume is by 1–2 orders of magnitude lower. Considering the perovskite to post-perovskite phase transition changes the situation in the slab areas in the CMB region. Let us consider first, that the viscosity of the post-perovskite is constant and equal to 10^{21} Pa s (Fig. 3b). Compared to the previous model, the viscosity

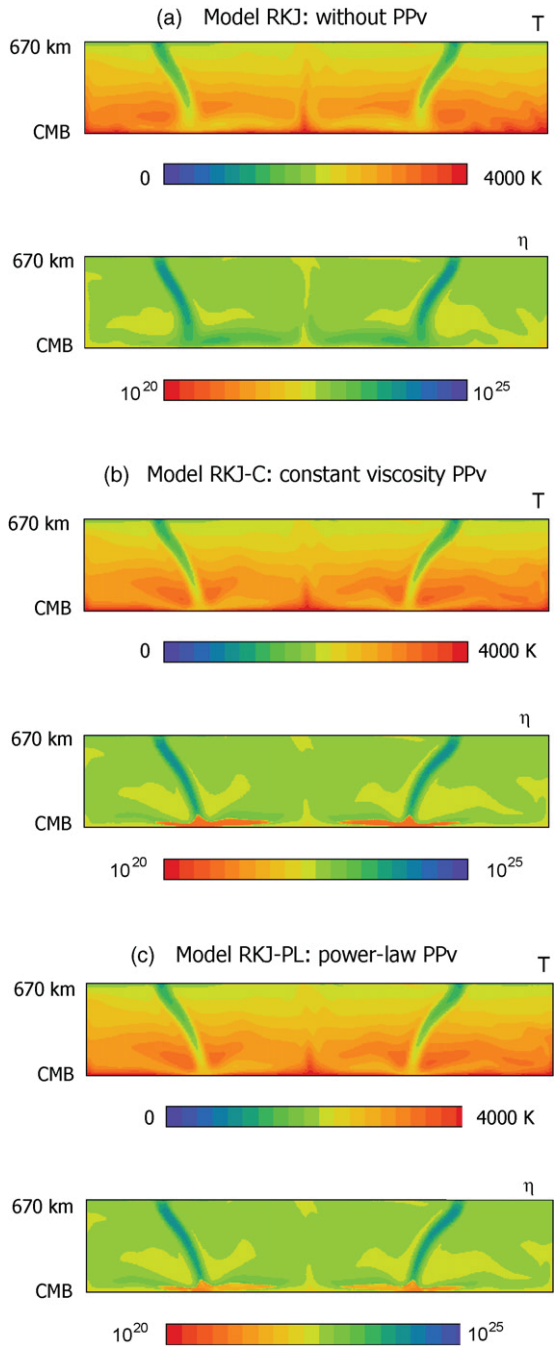

Fig. 3. The distribution of the temperature (upper row) and viscosity (lower row) at a time 350 Myr. (a) Model RKJ without post-perovskite phase transition. (b) Model RKJ-C with a constant viscosity post-perovskite ($\eta_{PPv} = 10^{21}$ Pa s). (c) Model RKJ-PL with power-law rheology of post-perovskite.

distribution in the CMB region has changed considerably. We still have a plume in the middle of the model box with the viscosity of about 10^{22} Pa s, but now it is surrounded by two low-viscosity post-perovskite lenses. The weak post-perovskite just above the CMB can spread easily, which results in a more symmetric pattern of the cold anomalies at the bottom of the mantle. There are no 'hockey sticks' in this case and the cold anomaly associated with the flat-lying slab material is considerably smaller than that in model RKJ shown in Fig. 3a. The temperature contrast between the central plume and the ambient mantle is almost negligible in the mid-lower mantle and, therefore, relatively low viscosities are present only in the root and the head of the plume. If we take a more complex model of the post-perovskite deformation (power-law, model RKJ-PL), we obtain similar results (Fig. 3c). Despite the fact that the effective viscosity within the post-perovskite lenses is somewhat higher than in the case shown in Fig. 3b, the dynamics of the model is almost the same.

Though little observational evidence is available to constrain the lowermost mantle flow, some information can be retrieved from the seismic observations. The model of the lowermost mantle seismic anisotropy (Panning and Romanowicz, 2006) shows that in the circum-Pacific regions the horizontally polarized S-wave is faster than the vertically polarized one ($v_{SH} > v_{SV}$). It has been shown by Mcnamara et al. (2001); Mcnamara (2003), that the localization of the dislocation creep in the bottom layer of the perovskite mantle under the slabs may produce the necessary LPO, but it cannot explain the amplitude of the anisotropy (Shim, 2008). This, however, may be attributed to post-perovskite, which should be present in these presumably cold areas below subduction zones (e.g. Oganov and Ono, 2004; Shim, 2008). The role of post-perovskite in explaining the observed lowermost mantle anisotropy is not yet completely clear due to the disagreement about the correct slip system for post-perovskite (Wookey and Kendall, 2007). Yamazaki and Karato (2001) suggest, that the D'' anisotropy can be explained by the LPO of the mixture of post-perovskite and ferropericlase associated with the horizontal shear flow. In Fig. 4 we show the flow in the lowermost part of our model domain in the model RKJ without post-perovskite (upper panel) and in the model RKJ-PL with a power-law rheology of post-perovskite (lower panel). Both panels show a close-up of the bottom part of the downwelling slab. The arrows indicating the flow velocity are plotted over the viscosity distribution. The orange structure in the bottom panel is the weak post-perovskite lens. Clearly the horizontal shear flow, that is needed for the LPO generation, develops in the model with a weak power-law post-perovskite.

The presence of the low-viscosity post-perovskite at the base of the model changes the geotherm in the lowermost mantle. Fig. 5 shows the average geotherms for the models shown in Fig. 3: RKJ (solid line) and RKJ-PL (dashed line). Both are plotted for the depths below 2000 km. The geotherm for the model RKJ-C is not plotted here—it is very close to the dashed line and the model RKJ-PL. The distribution of the average temperature in both models is very close to each other up to the depth of about 2200 km and their gradient is approximately adiabatic. Below that depth (above the D'') both geotherms are substantially subadiabatic. Similar to the results of Nakagawa and Tackley (2004); Tackley et al. (2007), the geotherm of model with power-law post-perovskite (RKJ-PL) is warmer than that of the model without post-perovskite (RKJ) by more than 100 K. The model including low-viscosity post-perovskite shows also a steeper increase of tem-

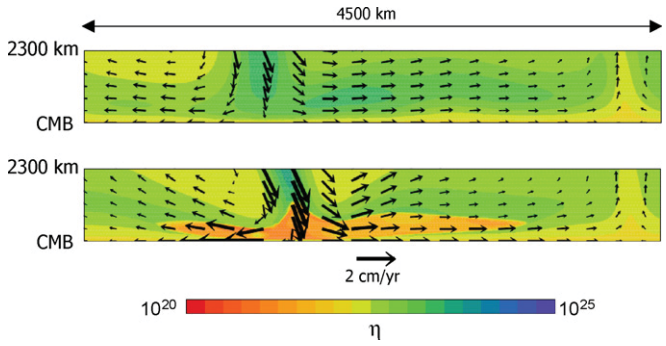

Fig. 4. Close-up of the model domain at the foot of the slab. Color marks the viscosity, arrows show the flow velocity. Upper panel: model RKJ without post-perovskite; lower panel: model RKJ-PL with power-law rheology of post-perovskite.

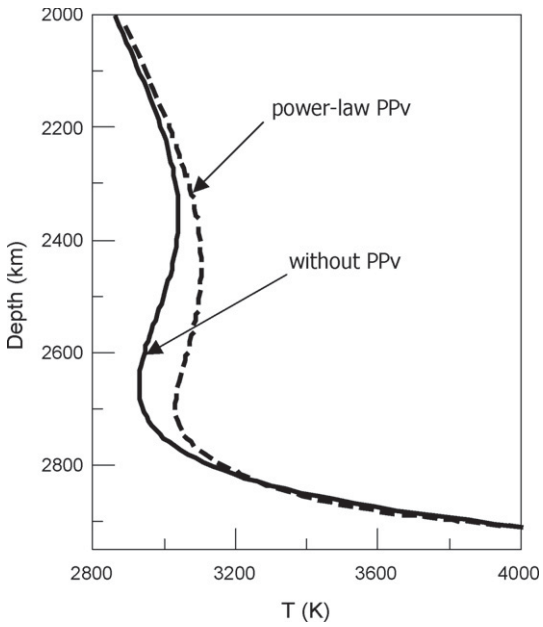

Fig. 5. Average geotherms for the models shown in Fig. 3. Solid line corresponds to the model RKJ without post-perovskite, the dashed line is for the model RKJ-PL with power-law post-perovskite.

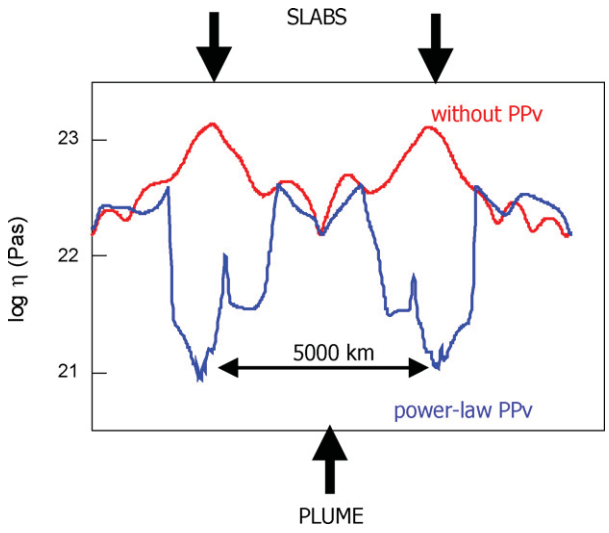

Fig. 6. Lateral changes of viscosity taken 80 km above the CMB. Red curve is for the model without post-perovskite (RKJ), blue curve for the model with power-law post-perovskite (RKJ-PL). The black arrows indicate the position of the slabs and plume in the model. (For interpretation of the references to color in this figure legend, the reader is referred to the web version of the article.)

perature in the CMB region, thus indicating an increased heat flux from the core.

The motivation for this work came from the inversion of the geoid by Čadek and Fleitout (2006) predicting low viscosity under the cold downwellings and higher than average viscosity under the hotspots. Fig. 6 illustrates the lateral viscosity variations 80 km above the CMB in the models without and with the post-perovskite phase change. In the model RKJ without post-perovskite the viscosity maxima are located under the slabs, while the low viscosity is obtained in the plume area (red line). If the post-perovskite with a power-law creep is considered (model RKJ-PL) we indeed get an inverse viscosity distribution with the low viscosity in the cold post-perovskite slabs and a relatively high viscosity in the warm perovskite plume (blue line).

So far we have concentrated on the models with an intercept temperature of 3500 K. Let us now look at the influence of the intercept temperature on the dynamics of the CMB region. Fig. 7 shows the results obtained for the models with power-

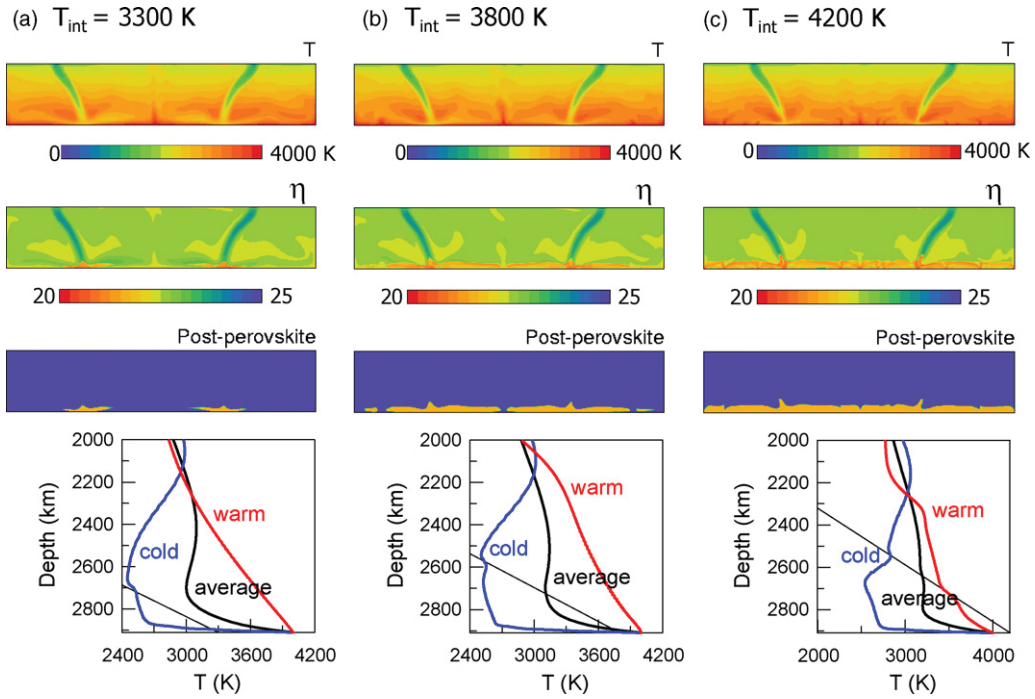

Fig. 7. Temperature (first row), viscosity (second row), the distribution of post-perovskite (third row) and the geotherms together with the Clapeyron curve (fourth row) obtained in three models with different intercept temperature: (a) T_{int}=3300 K, (b) T_{int}=3800 K and (c) T_{int}=4200 K. The cold (blue) geotherm taken through the slab, warm geotherm (red) taken through the plume and the average geotherm (black) are shown. The Clapeyron slope of 9 GPa/K is applied in all these models. Post-perovskite is deformed via dislocation creep. The activation parameters set RKJ-PL is assumed for perovskite and post-perovskite. (For interpretation of the references to color in this figure legend, the reader is referred to the web version of the article.)

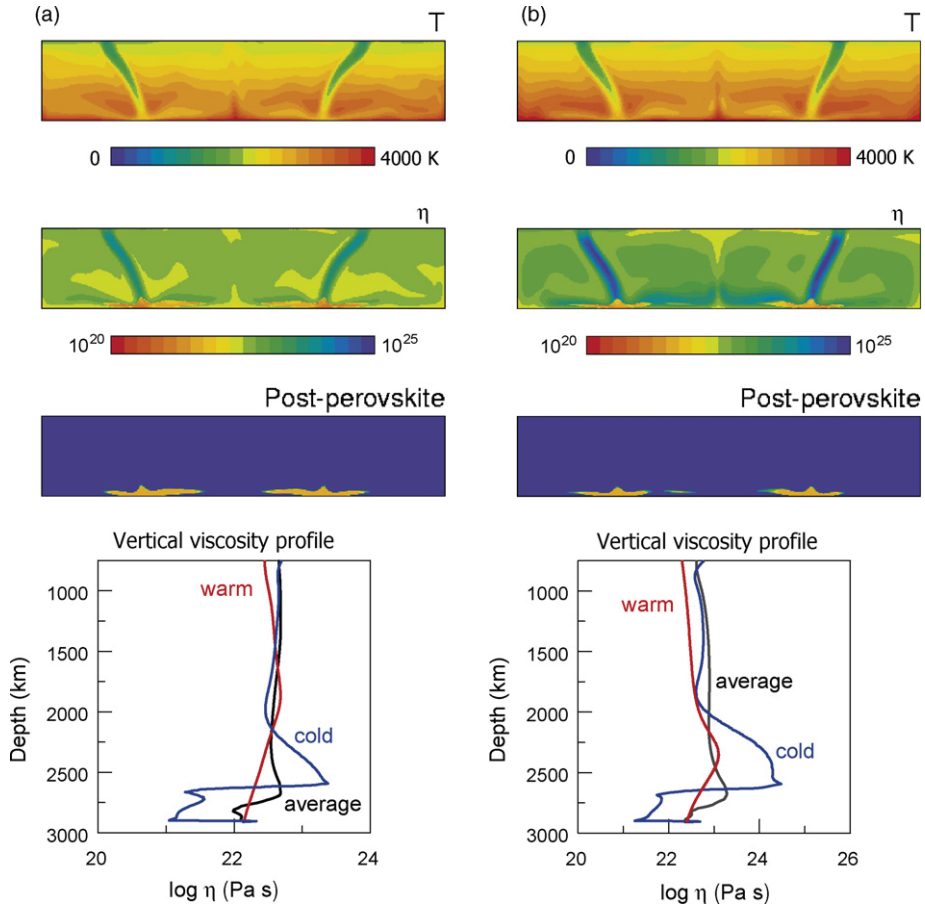

Fig. 8. Temperature (first row), viscosity (second row), the distribution of post-perovskite (third row) and the vertical profile of viscosity in two models with different activation parameters of perovskite and post-perovskite. Viscosity profiles are taken through a cold slab (blue line), through a warm plume (red line) and an average profile is also shown (black line). (a) Model RKJ-PL, (b) Model RYK-PL (see Table 1). (For interpretation of the references to color in this figure legend, the reader is referred to the web version of the article.)

law creep in post-perovskite (rheological model RKJ-PL) and for the three values of the intercept temperature: 3300 K (panel a), 3800 K (panel b) and 4200 K (panel c). In the case of the low intercept temperature the average geotherm (black line) lies above the Clapeyron curve (Fig. 7a, bottom row) and the post-perovskite thus appears only in the coldest parts of the model (cold geotherm—blue line). The lenses here are smaller than in the previously discussed model with $T_{int} = 3500$ K (cf. Fig. 3c), but the dynamics of these models is similar. If a higher intercept temperature of 3800 K is considered (Fig. 7b), the average geotherm has a double crossing with the Clapeyron curve. In this model we observe large lenses of post-perovskite, forming almost a continuous layer. The presence of the low viscosity material at the CMB enhances the activity of small plumes (lower left and lower right corners of the box), but there is still one larger plume in the middle of the box. In the third model (panel c) the intercept temperature is higher than the CMB temperature and the continuous layer of post-perovskite is formed. The cold anomaly associated with the slabs in the lowermost mantle is rather weak in this case, so the temperature at the foot of the geotherm is higher here compared to the models shown in Fig. 7a and b. Between the slabs, in the middle of the box, we find a swarm of small-scale plumes, rather than one strong plume as in the previously discussed models.

Since the rheological parameters of neither perovskite nor post-perovskite are well constrained, we tested the influence of the rheological parameters on the dynamics of the lowermost mantle. Fig. 8 compares the results obtained for the rheological model RKJ-PL with those reached for the model RYK-PL with the higher value of the activation parameters. In both models the intercept temperature was 3500 K. Panel a shows the results for the lower value of the activation parameters (the same model as shown in Fig. 3c). The horizontally averaged viscosity (bottom row in panel a Fig. 7, black line) does not change substantially over the lower mantle (it is about 10^{22} Pa s) except for the bottom boundary layer, where it drops by about an order of magnitude due to the presence of the weak post-perovskite. The rheological model RYK-PL (panel b Fig. 7) yields a stiffer lower mantle (cf. Fig. 8a and b, second row). The horizontally averaged viscosities are now about a factor 5 higher than in the previous case (Fig. 8b, fourth row). The temperature distribution is slightly different—the geotherm in the lower part of the model domain is warmer, but the basic dynamic characteristics of the models Fig. 8a and b are similar.

As we already mentioned above, the presence of the weak post-perovskite in the bottom boundary layer has important consequences for the average geotherm above the CMB. We shall now look at the heat flux evolution in some of the models discussed above. In Fig. 9a we show the average heat flux at the CMB as a function of time for the models with the constant viscosity post-perovskite. The intercept temperature in all three models shown here is 3500 K. In the model without post-perovskite (red line) the heat flux is increasing slowly at the beginning of the calculation as the slab is descending through the mantle. At a time slightly over 100 Myr, when the slabs reach the bottom of the mantle, the heat flux increases faster and then remains more or

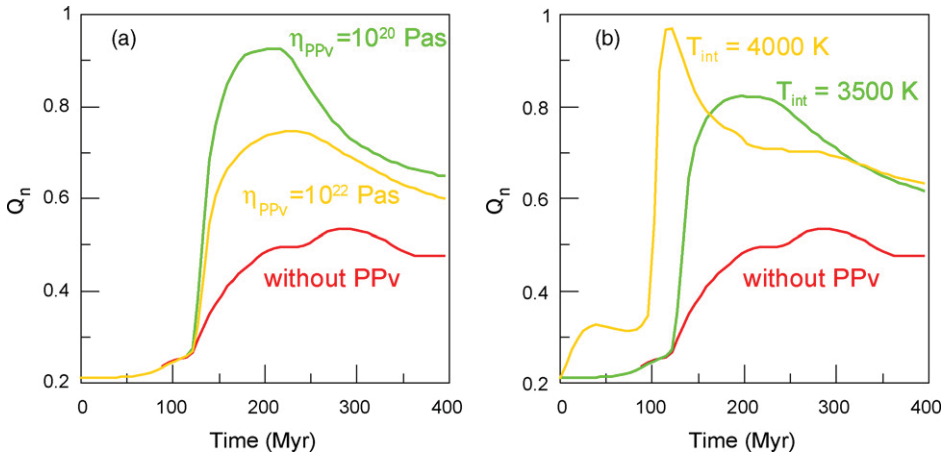

Fig. 9. Time evolution of the heat flux across the CMB. (a) Models with constant viscosity post-perovskite and intercept temperature 3500 K. (b) Models with the power-law post-perovskite (model RKJ-PL) and various intercept temperatures. Heat flux is normalized by its maximum value.

less constant. If the post-perovskite phase transition is considered with the post-perovskite viscosity of 10^{22} Pa s (yellow line), the heat flux increase is much more rapid after the slabs reach the CMB. The low viscosity areas in the lower boundary layer enhance the heat flux considerably. If the post-perovskite viscosity is yet lower (10^{20} Pa s, green line), the heat flux increase is even higher. In the presence of the isolated lenses of a low-viscosity post-perovskite, the average heat flux at the CMB could vary by about a factor of 1.5–2 depending on the post-perovskite viscosity. Fig. 9b shows the evolution of the CMB heat flux as a function of the intercept temperature for the power-law creep post-perovskite (rheological model RKJ-PL). The average heat flux increases now with the intercept temperature—the more post-perovskite we have in the bottom boundary layer, the higher the heat flux is.

The details of the CMB heat flux are further illustrated in Fig. 10. Here we plot the normalized heat flux along the CMB at one time instant (taken after 350 Myr evolution from the initial state) for several models with different intercept temperatures. The model RKJ without post-perovskite (dashed orange line) has a minimum in the middle of the box, where the plume is located (cf. Fig. 3a) and two maxima associated with the cold feet of the two slabs. When the weak post-perovskite lenses with the temperature intercept of 3500 K are present (purple solid line), the heat flux peaks in the cold slab areas are by about a factor of 2 higher than in the model with strong perovskite slabs (orange dashed line). With yet higher intercept temperatures there is more post-perovskite in the bottom boundary layer and the heat flux maxima grow higher (by up to a factor 3—dark blue and light blue solid lines).

Finally, we have tested the effect of the lower CMB temperature to our results ($T_{CMB} = 3800$ K and $T_{CMB} = 3500$ K). We can generally conclude that the flow situation does not change considerably except perhaps slightly thicker and more sluggish plumes. What concerns the CMB heat flux, the curves for the lower CMB temperatures are rather similar to the curves shown in Fig. 10—assuming the low viscosity power-law creep for post-perovskite greatly enhances the peaks of the CMB heat flux under the cold slabs.

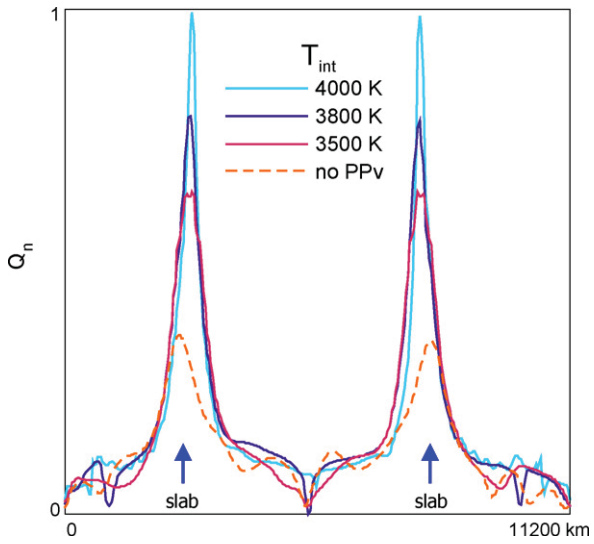

Fig. 10. Normalized heat flux along the CMB at one time instant (taken after 350 Myr evolution from the initial state) for several models with different intercept temperatures. Arrows indicate the location of the slabs.

4. Conclusions

We have shown that the concept of weak post-perovskite lens surrounded by relatively stiff perovskite plumes which could explain the viscosity paradox suggested by the geoid inversion (Čadek and Fleitout, 2006) is dynamically feasible. We tested two different models of activation parameters for perovskite (Knittle and Jeanloz, 1987; Yamazaki and Karato, 2001) and found that the shape of the post-perovskite lens as well as the dynamic regime of the D'' layer do not depend much on the rheological model of perovskite. The rheological description of post-perovskite (constant viscosity vs. power-law) and its actual effective viscosity do not play an important role either, provided the post-perovskite is weaker than perovskite.

The dynamics of the D'' layer is strongly influenced by the parameters of the perovskite to post-perovskite phase transition, namely by the temperature intercept. If T_{int} is in the range 3300–3800 K, the post-perovskite forms the isolated patches. Regardless their size, the flow character is rather similar—the two cold slabs are separated by one plume formed in between. The adopted rheological model of perovskite results in the creation of the central plume, which is in terms of viscosity "almost invisible" in the mid-lower mantle. The situation changes only if the intercept temperature is higher than the CMB temperature. Then the post-perovskite forms a continuous layer at the bottom of the mantle and its low viscosity gives rise to a swarm of small plumes rather then one big plume as in the previous cases. The horizontal shear flow developed in the weak post-perovskite lenses may explain the polarization anisotropy observed in the paleoslab areas in the lowermost mantle.

Ever since the post-perovskite phase transition was discovered, the effect of post-perovskite to the CMB heat flux and the core–mantle coupling has widely been discussed (Nakagawa and Tackley, 2004, 2008; Buffett, 2007; van der Hilst et al., 2007; Lay et al., 2008). Nakagawa and Tackley (2004, 2008) discuss the effects of post-perovskite phase transition on the CMB heat flux in the models of thermal and thermo-chemical convection and conclude, that the deep exothermic phase change enhances heat transport. Further, they show that the peak-to-peak lateral variations of the CMB heat flux generate the heat flux ratio $q^* = (q_{\max} - q_{\min})/(2q_{average})$ higher than 1, which may be potentially problematic for the dynamo generation (Olson and Christensen, 2002). In their models the post-perovskite has the same rheology as perovskite. Here we show that the presence of the rheologically weak post-perovskite in the CMB region decreases the thickness of the bottom boundary layer and strongly enhances the core–mantle heat flux in the cold areas below the slabs. Thus it should further increase the heat flux ratio q^*, which could have an impeding effect to the core dynamo action. We should note here, however, that our model concentrates on the local effect of the weak post-perovskite in the cold slab areas. Thus most of our model domain is occupied by the cold downwellings and our results cannot be representative for the global heat flux characteristics. Further, we should emphasize that our heat flux maximum is rather narrow and its wavelength is therefore not comparable with the relatively long wavelength heat flow pattern considered in the laminar regime dynamo studies (Christensen and Olson, 2003).

As the rheology of post-perovskite influences considerably the shape of post-perovskite lens, character of the lowermost mantle flow and the CMB heat flux, the new mineral physics constraints on the rheological parameters of the post-perovskite are crucial for further understanding of the lowermost mantle dynamics.

Acknowledgements

We thank Artem Oganov and Arie van den Berg for fruitful discussions and two anonymous reviewers for the comments that helped to improve the manuscript. This work was supported by the Research Program MSM0021620860 of the Ministry of Education, by the Charles University Grant Agency (GAUK 2333/2007) and by the MCRTN project "c2c: The fate of subducted material". D.A. Yuen acknowledges support from the VLAB grant due to ITR program of the National Science Foundation.

References

Buffett, B.A., 2007. A bound on heat flow below a double crossing of the perovskite–postperovskite phase transition. Geophys. Res. Lett. 34, L17302. doi:10.1029/2007GL030930.

Čadek, O., Fleitout, L., 2006. Effect of lateral viscosity variations in the core–mantle boundary region on predictions of the long-wavelength geoid. Stud. Geophys. Geod. 50, 217–232.

Carrez, P., Ferre, D., Cordier, P., 2007. Implications for plastic flow in the deep mantle from modelling dislocations in $MgSiO_3$ minerals. Nature 7131, 68–70.

Christensen, U., Olson, P., 2003. Secular variation in numerical geodynamo models with lateral variations of boundary heat flow. Phys. Earth Planet. Int. 138, 39–54.

Forte, A.M., Mitrovica, J.M., 2001. Deep-mantle high-viscosity flow and thermochemical structure inferred from seismic and geodynamic data. Nature 410, 1049–1056.

Forte, A.M., Mitrovica, J.X., Espesset, A., 2002. Geodynamic and seismic constraints on the thermochemical structure and dynamics of convection in the deep mantle. Philos. Trans. Roy. Soc. Lond., Ser. A: Math. Phys. Eng. Sci. 360, 2521–2543.

Hernlund, J.W., Thomas, C., Tackley, P.J., 2005. A doubling of the post-perovskite phase boundary and structure of the Earth's lowermost mantle. Nature 7035, 882–886.

Hirose, K., Lay, T., 2008. Discovery of post-perovskite and new views on the core–mantle boundary region. Elements 3, 183–189.

Ishii, M., Tromp, J., 1999. Normal-mode and free-air gravity constraints on lateral variations in velocity and density of Earth's mantle. Science 285, 1231–1236.

Ita, J., King, S.D., 1994. Sensitivity of convection with an endothermic phase change to the form of governing equations, initial conditions, boundary conditions, and equation of state. J. Geophys. Res. 99, 15919–15938.

Karato, S., 1998. Seismic anisotropy in the deep mantle, boundary layers and the geometry of mantle convection. Pure Appl. Geophys. 151, 565–587.

Karato, S., Karki, B.B., 2001. Origin of lateral variation of seismic wave velocities and density in the deep mantle. J. Geophys. Res. 106 (B10), 21771–21783.

Karato, S., Zhang, S.Q., Wenk, H.R., 1995. Superplasticity in the lower mantle—evidence from seismic anisotropy and rock physics. Science 270, 458–461.

Knittle, E., Jeanloz, R., 1987. The activation energy of the back transformation of silicate perovskite to enstatite. In: Manghnani, M., Syono, Y., (Eds.), High-Pressure Research in Mineral Physics, 243–250.

Lay, T., Hernlund, J., Buffett, B.A., 2008. Core–mantle boundary heat flow. Nat. Geosci. 1, 25–32.

Masters, G., Laske, G., Gilbert, F., 2000. Matrix autoregressive analysis of free-oscillation coupling and splitting. Geophys. J. Int. 143, 478–489.

Mcnamara, A.K., Karato, S.I., van Keken, P.E., 2001. Localization of dislocation creep in the lower mantle: implications for the origin of seismic anisotropy. Earth Planet. Sci. Lett. 191, 85–99.

Mcnamara, A.K., van Keken, P.E., Karato, S.I., 2003. Development of finite strain in the convecting lower mantle and its implications for seismic anisotropy. J. Geophys. Res. 108, 2230. doi:10.1029/2002JB001970.

Murakami, M., Hirose, K., Kawamura, K., Sata, N., Ohishi, Y., 2004. Post-perovskite phase transition in $MgSiO_3$. Science 7, 855–858.

Nakagawa, T., Tackley, P.J., 2004. Effects of a perovskite-post perovskite phase change near core–mantle boundary in compressible mantle convection. Geophys. Res. Lett. 31, L16611. doi:10.1029/2004GL020648.

Nakagawa, T., Tackley, P.J., 2008. Lateral variations in CMB heat flux and deep mantle seismic velocity caused by a thermal-chemical-phase boundary layer in 3D spherical convection. Earth Planet. Sci. Lett. 271, 348–358.

Oganov, A., Ono, S., 2004. Theoretical and experimental evidence for a post-perovskite phase of $MgSiO_3$ in Earth's D''. Nature 430, 445–448.

Oganov, A., Ono, S., 2005. The high pressure phase of alumina and implications for earth's D'' layer. Proc. Natl. Acad. Sci. 102, 10828–10831.

Ohta, K., Onoda, S., Hirose, K., Sinmyo, R., Shimizu, K., Sata, N., Ohishi, I., Yasuhara, A., 2008. The electrical conductivity of post-perovskite in Earth's D'' layer. Science 320, 89–91.

Olson, P., Christensen, U., 2002. The time-averaged magnetic field in numerical dynamos with non-uniform boundary heat flow. Geophys. J. Int. 151, 809–823.

Ono, S., Oganov, A., Koyama, T., Shimizu, H., 2006. Stability and compressibility of the high-pressure phases of Al_2O_3 up to 200 GPa: implications for the electrical conductivity of the base of the lower mantle. Earth Planet. Sci. Lett. 246, 326–335.

Panning, M., Romanowicz, B., 2006. A three-dimensional radially anisotropic model of shear velocity in the whole mantle. Geophys. J. Int. 167, 361–379.

Riedel, M.R., Karato, S., 1997. Grain-size evolution in subducted oceanic lithosphere associated with the olivine–spinel transformation and its effects on rheology. Earth Planet. Sci. Lett. 148, 27–43.

Segal, A., Praagman, N. P., 2005. The sepran fem package. Technical report, Ingenieursbureau Sepra, The Netherlands. http://ta.twi.tudelft.nl/sepran/sepran.html.

Shim, S.H., 2008. The post-perovskite transition. Ann. Rev. Earth Planet. Sci. 36, 569–599.

Solomatov, V.S., 1996. Can hotter mantle have a larger viscosity? Geophys. Res. Lett. 23, 937–940.

Solomatov, V.S., El-Khozondar, R., Tikare, V., 2002. Grain size in the lower mantle: constraints from numerical modeling of grain growth in two-phase systems. Phys. Earth Planet. Int. 129, 265–282.

Tackley, P.J., Nakagawa, T., J.W. Hernlund, 2007. influence of the post-perovskite transition on thermal and thermo-chemical mantle convection. In: Post-Perovskite: The Last Mantle Phase Transition, Geophys. Monogr. Ser. vol. 174, 229–247.

Tosi, N., Čadek, O., Martinec, Z., Yuen, D.A., Kaufmann, G., 2009. Is the long-wavelength geoid sensitive to the presence of post-perovskite above the core–mantle boundary? Geophys. Res. Lett. 36. doi:10.1029/2008GL036902.

Tsuchiya, T., Tsuchiya, J., Umemoto, K., Wentzcovitch, R.M., 2004. Phase transition in MgSiO3 perovskite in the earth's lower mantle. Earth Planet. Sci. Lett. 224, 241–248.

van Hunen, J., van den Berg, A.P., Vlaar, N.J., 2000. A thermo-mechanical model of horizontal subduction below an overriding plate. Earth Planet. Sci. Lett. 182, 157–169.

van Hunen, J., van den Berg, A.P., Vlaar, N.J., 2004. Various mechanisms to induce present-day shallow flat subduction and implications for the younger earth: a numerical parameter study. Phys. Earth Planet. Int. 146, 179–194.

van den Berg, A.P., van Keken, P.E., Yuen, D.A., 1993. The effects of a composite non-Newtonian and Newtonian rheology on mantle convection. Geophys. J. Int. 115, 62–78.

van der Hilst, R., Hoop, M.D., Wang, S., Shim, L., Tenorio, P., 2007. Seismo-stratigraphy and thermal structure of Earth's core–mantle boundary region. Science 315, 1813–1817.

Walte, N., Heidelbach, F., Miyajima, N., Frost, D., 2007. Texture development and TEM analysis of deformed $CaIrO_3$: implications for the D00 layer at the core–mantle boundary. Geophys. Res. Lett. 34. doi:10.1029/2007GL029407.

Wookey, J., Kendall, J.-M., 2007. Seismic anisotropy of post-perovskite and the lowermost mantle. In: Post-Perovskite: The Last Mantle Phase Transition, Geophys. Monogr. Ser. 174, 171–189.

Yamazaki, D., Karato, S., 2001. Some mineral physics constraints on rheology and geothermal structure of earth's lower mantle. Am. Miner. 86, 358–391.
Yamazaki, D., Kato, T., Ohtani, E., Toriumi, M., 1996. Grain growth rates of $MgSiO_3$ perovskite and periclase under lower mantle conditions. Science 274, 2052–2054.
Yamazaki, D., Yoshino, T., Ohfuji, H., Ando, J., Yoneda, A., 2006. Origin of seismic anisotropy in the D'' layer inferred from shear deformation experiments on post-perovskite phase. Earth Planet. Sci. Lett. 252, 372–378.
Yamazaki, D., Karato, S., 2007. Lattice preferred orientation of lower mantle materials and seismic anisotropy in the D" layer. In: Post-Perovskite: The Last Mantle Phase Transition, Geophys. Monogr. Ser. vol. 174, 69–78.
Yuen, D.A., Matyska, C., Čadek, O., Kameyama, M., 2007. The dynamical influences from physical properties in the lower mantle and post-perovskite phase transition. In: Post-Perovskite: The Last Mantle Phase Transition, Geophys. Monogr. Ser. vol. 174, 249–270.